Mon. Not. R. Astron. Soc. **000**, ??–?? (2010) Printed 24 November 2010 (MN LATEX style file v2.2)

Interstellar Dust Models towards some IUE Stars

Nisha Katyal[1⋆], Ranjan Gupta[1]†, D.B.Vaidya[2]‡

[1] *IUCAA, Post Bag 4, Ganeshkhind, Pune, 411007, India*
[2] *ICCSIR, Ahmedabad-380009, India*

Accepted. Received; in original form

ABSTRACT
We present a study of interstellar extinction towards certain directions in our galaxy defined by about 59 stars which were observed by the IUE satellite. The observed UV extinction curves have been modeled by making light scattering calculations based on Discrete Dipole Approximation (DDA) for extinction efficiencies of composite dust grains which is made up of a host silicate spheroid and graphite inclusions. The study indicates that smaller dust grains are more efficient for the directions in the galaxy where observed R_v values are found to be low.

Key words: Interstellar Dust, Extinction, Ultraviolet spectra

1 INTRODUCTION

Interstellar dust models have evolved with the advance of observational data. Before the advent of rocket-borne instruments and satellites the astronomical ultraviolet studies were not possible due to atmospheric extinction. In 1968, the first satellite, OAO2, capable of UV observations was launched, and later other satellites, viz. TD-1, Astronomy Netherland Satellite (ANS) and International Ultraviolet Explorer (IUE) were launched. We intend to study the wavelength dependence of interstellar extinction mainly in the UV region using the data of IUE (International Ultraviolet Explorer) which was launched in 1978. IUE has provided a wealth of data on interstellar extinction which has broadened our horizon for understanding the dust grain properties in various regions of interstellar medium. The low dispersion mode of IUE covers a wavelength range of 1153-3200 Å at a resolution of 6 Å . There have been previous studies with these UV satellites. Massa et al. (1983) have done spectrophotometric measurements for a sample of stars judged by Meyer & Savage (1981) to study highly anomalous peculiar UV extinction as inferred from the broad-band Astronomical Netherlands Satellite (ANS) data. Greenberg & Chlewicki (1983) have found strong correlation between strength of bump and visible extinction. Also they obtained poor correlation between far ultraviolet (FUV) extinction and either of bump and visible extinction concluding that a wide spectrum of size distribution is needed to explain the average observed interstellar extinction curve. Aiello et al. (1988) have presented a collection of 115 extinction curves derived from low dispersion IUE spectra. The atlas includes extinction originating in the diffuse medium and several major nebulae and dense clouds. We have used the methodology of Fitzpatrick & Massa (1986) and Fitzpatrick & Massa (1988) (henceforth FM) to employ a parameterization scheme for generation of extinction curves. Using this scheme, Fitzpatrick & Massa (1990) have displayed UV extinction curves and subsequently analysed the fits graphically. More recently Fitzpatrick & Massa (2005, 2007) presented a new method for deriving 328 galactic interstellar IR and UV extinction curves affecting normal, near main sequence B and late O type stars based on the use of stellar atmospheric models to provide estimates of the intrinsic (i.e. unreddened) stellar spectral energy distributions (SEDs), rather than unreddened (or lightly reddened) standard stars.

There are now ample number of observed extinction curves available in the literature. These are found to vary with different line of sights because of the prevailing interstellar conditions. Cardelli et al. (1988) (hereafter CCM) found this dependence on the interstellar environment can be well characterized by a single parameter $R_v = A(V)/E(B-V)$, the ratio of visual extinction to reddening. Kim et al. (1994) found out that denser environments with high R_v(=5.3) seem to be due to larger mean size of grains though all denser regions may not necessarily have high R_v. The shape of extinction curves are substantially different for different $R_v's$, and hence we expect changes in the size distributions as well. As Cardelli & Clayton (1991) have pointed out, lines of sight with large R_v are ideal for examining processes that modify the grain properties in dense clouds. Weingartner & Draine (2001)

⋆ E-mail: nishakat@iucaa.ernet.in
† E-mail: rag@iucaa.ernet.in
‡ E-mail: dipak.vaidya@gmail.com

have constructed size distributions for carbonaceous and silicate grain populations in different regions of the Milkyway, LMC and SMC to account for the observed IR and microwave emissions from diffuse interstellar medium. They have shown that these variations can be well parametrized by R_v. Most recently, Fitzpatrick & Massa (2009) did a general survey of Galactic extinction covering the Near IR (NIR) and have provided an alternative model by assuming a different i functional form of NIR extinction providing a much better fit to NIR extinction curves. Also, the observed normalised extinction k(K-V) and R_v derived from fits are seen strongly correlated. The interstellar grain models should be developed in a manner so that it satisfies the observations of interstellar abundances, extinction, composition of dust grains etc. Hence, we do a detailed analysis of the shapes of observed extinction curves and compare them with the model.

The main objective of the paper is to study the physical properties of the dust grains and its composition towards various sight lines. We use **DDSCAT6.1** (Discrete Dipole Scattering) code to study the light scattering phenomenon by dust grains. For description on DDA (Discrete Dipole Approximation) see Draine (1988). Irregular shape effects, surface roughness and internal structure within the grain are well considered by DDA (Wolff et al. 1994, 1998; Voshchinnikov et al. 2005). Clayton et al. (2003) have presented a uniform set of Maximum Entropy Method (MEM) model fits for extinction properties seen in the Galaxy and Magellanic clouds. They use homogeneous sphere grain models with two (graphite, silicate) or three (graphite, silicate, amorphous carbon) components. Voshchinnikov et al. (2006) apply the particle models of porous interstellar dust grains based on the EMT-Mie and layered sphere calculations and have evaluated the extinction curves towards directions of two stars using solar abundances. Further, they mention that DDA is required in treating particles with inclusions larger than the wavelength of incident radiation. We use a more realistic composite spheroidal grain model and calculate the extinction efficiencies in the wavelength range 0.55-0.10μm (Vaidya et.al. 2001).

Section II is divided into four subsections. Subsection 2.1 describes the 'Pair Method' used to generate the extinction curves for a set of IUE stars and subsection 2.2 describes an analytical FM method for generation of extinction curves for another set of IUE stars. In subsection 2.3, we discuss the selection criteria for the program stars along with their observed properties and in subsection 2.4, the procedure for the merging of the short and long wavelength bands from the IUE data is described. Section III provides the details of the composite DDA model. Section IV presents results and discussions followed with conclusions in Section V.

2 PRELIMINARY DATA REDUCTION

2.1 PAIR METHOD

The standard Pair method technique is used for a set of IUE stars (hereafter called Set I described in the section 2.3) to generate the extinction curves. The technique involves to select a highly reddened star and compare it with a star (flux standard) which has negligible reddening and whose spectral features closely match with those of the reddened star. An extinction curve is then constructed by the standard relation (Fitzpatrick & Massa (1988)):

$$\frac{E(\lambda - V)}{E(B - V)} = \frac{m(\lambda - V) - m(\lambda - V)_o}{(B - V) - (B - V)_o} \quad (1)$$

where subscript 'o' refers to the unreddened star and other is for the reddened star. Here E(B-V) is the difference in extinction between the specified wavelengths and corresponds to the colour excess. The resultant extinction curve $E(\lambda - V)/E(B - V)$ is then plotted versus $1/\lambda$ for selected IUE stars (Set I).

2.2 FM METHOD

For another set of IUE stars (hereafter called Set II described in section 2.3), we use an analytical method which parameterizes the observed UV extinction curves and is based on the empirical result which assumes that the entire UV extinction curve is well represented accurately by a combination of basic elements (Fitzpatrick & Massa 1988). Defining $x = \lambda^{-1}$, these elements are:

(i) a linear "background term", (ii) a Lorentzian like "Drude profile", $D(x, \gamma, x_0)$, which represents the 2175 Å bump and (iii) a far-UV curvature term, F(x).

The complete parametrized function is given by:

$$K(x - V) = \frac{E(\lambda - V)}{E(B - V)} \quad (2)$$

$$= c_1 + c_2 x + c_3 D(x; \gamma, x_0) + c_4 F(x), \quad (3)$$

For more details vide Fitzpatrick & Massa (1988).

Valencic et al. (2004) have assembled a homogeneous database of 417 ultraviolet (UV) extinction curves for reddened sight lines having IUE spectra. They find out the parameters normalized with respect to A(V). However, we have adopted a normalization with respect to E(B-V) and thus all the 'c' parameters which define the extinction curve have changed considerably. Using equation (3) we generate extinction curves normalized to E(B-V).

2.3 Object Selection Criteria

Set I:

We have selected 27 "program stars" (listed in Table 1) from Fitzpatrick & Massa (1988) and IUE spectral atlas by Wu et al. (1983). The spectral types for the 27 stars (listed in Table 1) were limited to those earlier than B9, with most of the stars having spectral classes in the range O3-B3. Massa et al. (1983) and Massa et al. (1984) give the identification of features useful in matching B stars near the main sequence.

The column (1) of Table 1 gives the HD number of the Program star, column (2) gives HD number of comparison star followed by their spectral types, column (3) and (4) give magnitude in V and B band respectively, column (6) gives E(B-V) values and column (7) gives the value of observed R_v.

Figure 1 & 2 show the extinction curves for the 27 program stars.

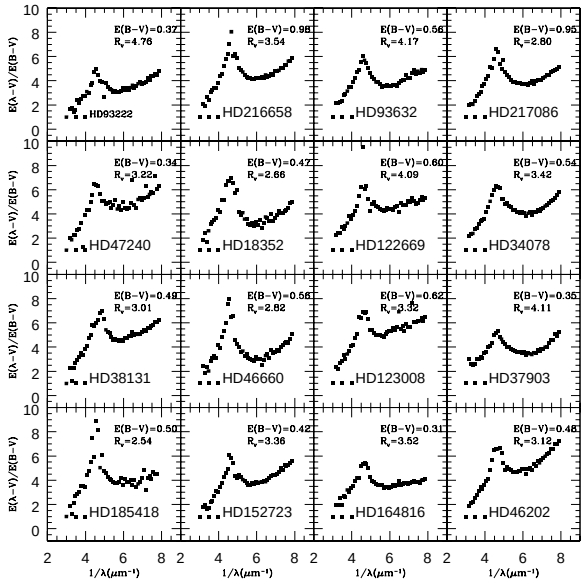

Figure 1. The figure displays the extinction curves for the program stars (Set I) obtained using the the "Pair Method".

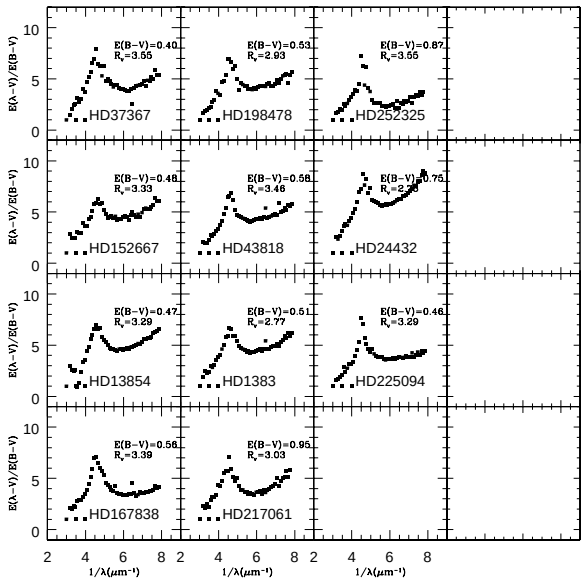

Figure 2. Same as Figure 1.

Set II:

We have also added another set of 32 stars in our analysis for which the parameters were obtained from Valencic et al (2004) and this list is given in Table 3. Figures 3 & 4 display the extinction curves for these 32 stars.

Table 2 provides the observational data for the flux standards i.e the comparison stars and table 3 provides the observational data for FM stars (Set II).

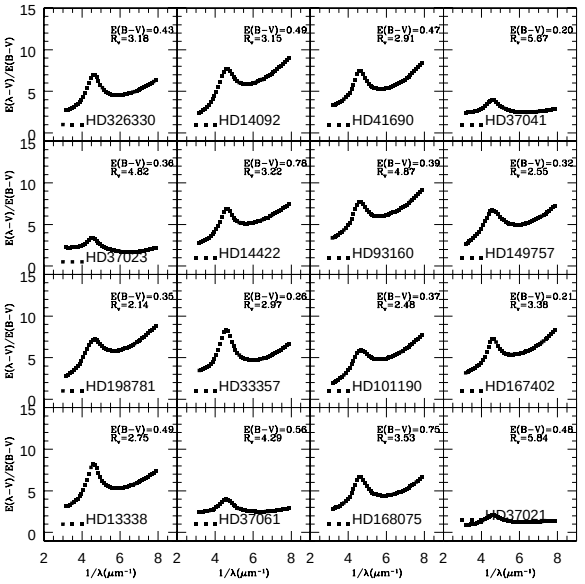

Figure 3. The figure displays the extinction curves for the program stars (Set II) obtained using the the "FM Method".

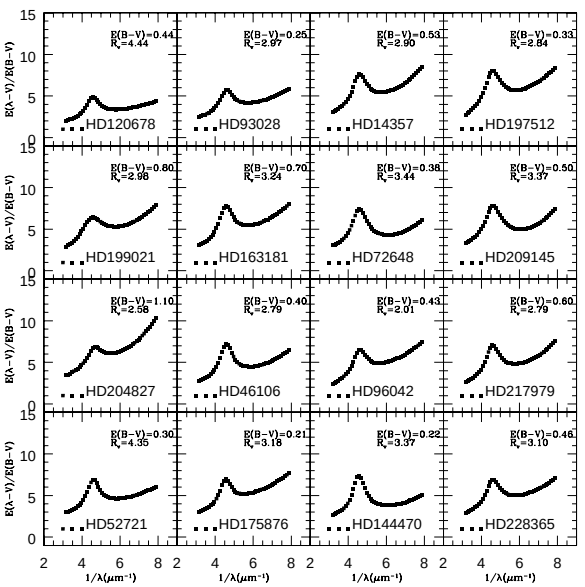

Figure 4. Same as Figure 3.

2.4 Merging of spectral bands for Pair Method

Each spectra of program star (Set I) consisted of two separate images, one for the shorter wavelength and another for the longer wavelength. Data was taken from following cameras: Short Wavelength Prime (SWP,$1150 < \lambda < 1978$ Å), Long Wavelength Redundant (LWR,$1851 < \lambda < 3348$ Å) and Long Wavelength Prime (LWP,$1851 < \lambda < 3347$ Å). For each program star, SWP and LWR/LWP data for fluxes was merged to achieve the instrumental resolution and the resultant fluxes were converted to magnitudes $m(\lambda)$, with λ

Table 1. Extinction curve data for program stars (Set I).

HD # (Sp Type)	Flux Std (Sp Type)	V	B	B-V	E(B-V)	R_v
93222 (O7IIIf)	47839 (O7 Vf)	8.10	8.15	0.05	0.37	4.76
47240 (B1 I)	91316 (B1 Iab)	6.18	6.26	0.08	0.34	3.22
38131 (B0.5V)	55857 (B0.5 V)	8.19	8.40	0.21	0.49	3.01
185418 (B0.5V)	55857 (B0.5 V)	7.45	7.67	0.22	0.50	2.54
216658 (B0.5V)	55857 (B0.5 V)	8.89	9.59	0.70	0.98	3.14
18352 (B1 V)	31726 (B1 V)	6.80	7.03	0.23	0.47	2.66
46660 (B1 V)	31726 (B1 V)	8.04	8.35	0.31	0.56	2.82
152723 (O7 V)	47839 (O7 Vf)	7.31	7.41	0.10	0.42	3.36
93632 (B0 V)	36512 (B0 V)	8.31	8.55	0.24	0.56	4.17
122669 (B0 V)	36512 (B0 V)	8.96	9.30	0.34	0.60	4.09
123008 (B0 V)	36512 (B0 V)	8.79	9.15	0.36	0.62	3.32
164816 (B0 V)	36512 (B0 V)	7.11	7.12	0.01	0.31	3.52
217086 (O7 V)	47839 (O7 Vf)	7.65	8.28	0.63	0.95	2.80
34078 (O9.5V)	38666 (O9.5 V)	5.99	6.18	0.19	0.54	3.42
37903 (B1.5V)	74273 (B1.5 V)	7.84	7.91	0.07	0.35	4.11
46202 (O9 V)	38666 (O9.5 V)	8.20	8.36	0.16	0.48	3.12
37367 (B2.5V)	192685 (B2.5 V)	5.98	6.11	0.13	0.40	3.55
152667 (B0.5I)	64760 (B0.5 V)	6.18	6.38	0.20	0.48	3.33
13854 (B1 Iab)	91316 (B1 I)	6.47	6.75	0.28	0.47	3.29
167838 (B5.0I)	58350 (B5 V)	6.74	7.10	0.36	0.56	3.39
198478 (B3.0I)	53138 (B3 Ia)	4.85	5.16	0.31	0.53	2.93
43818 (B0 II)	63922 (B0 III)	6.91	7.20	0.29	0.58	3.46
1383 (B1 II)	50707 (B1 II)	7.63	7.90	0.27	0.51	2.77
217061 (B1 V)	31726 (B1 V)	8.77	9.46	0.69	0.95	3.03
252325 (B1 V)	31726 (B1 V)	10.79	11.36	0.57	0.87	3.55
24432 (B3 II)	79447 (B3 III)	6.93	7.51	0.58	0.51	2.77
225094 (B3 Iab)	53138 (B3 Ia)	6.24	6.57	0.33	0.46	3.29

Table 2. Observational data for Flux standard stars.

HD #	Sp type	V	B	B-V	E(B-V)
47839	O7 Vf	4.65	4.41	-0.24	0.08
91316	B1 Iab	3.85	3.71	-0.14	0.05
55857	B0.5 V	6.11	5.85	-0.26	0.02
31726	B1 V	6.15	5.94	-0.21	0.05
36512	B0 V	4.62	4.36	-0.26	0.04
38666	O9.5 V	5.17	4.89	-0.28	0.02
74273	B1.5 V	5.87	5.69	-0.18	0.03
192685	B2.5 V	4.75	4.59	-0.16	0.05
64760	B0.5 V	4.23	4.08	-0.15	0.06
91316	B1 I	3.84	3.69	-0.15	0.05
58350	B5 V	2.40	2.37	-0.03	0.00
63922	B0 III	4.11	3.92	-0.19	0.11
50707	B1 II	4.82	4.66	-0.16	0.04
31726	B1 V	6.14	5.93	-0.21	0.05
79447	B3 III	3.96	3.77	-0.19	0.01
53138	B3 Ia	3.03	2.91	-0.12	0.04

covering the wavelength range 1150-3348Å . The magnitudes were further interpolated in the range 1153-3201Å with a binning of 1Å , and subsequently, the extinction curves were generated using standard Pair method discussed in Section 2.1.

3 DISCRETE DIPOLE APPROXIMATION (DDA) AND COMPOSITE GRAINS

The discrete dipole approximation (DDA) proposed by Purcell & Pennypacker (1973) allows for the computation of the optical properties of arbitrary shape particles. The basic DDA method consists of replacing a particle by an array of N oscillating polarizable point dipoles Draine (1988). The dipoles are located on a lattice and the polarizability is related to the complex refractive index $m = n + ik$ through a lattice dispersion relationship Draine & Goodman (1993).

Table 3. Extinction curve data for FM stars (Set II).

HD # (Sp Type)	V	B	E(B-V)	R_v
326330 (B0.5 V)	9.63	9.81	0.43	3.18
37023 (B0.5 V)	6.69	6.77	0.36	4.82
198781 (B0.5 V)	6.45	6.52	0.35	2.14
13338 (B1 V)	8.08	8.14	0.49	2.75
37061 (B1 V)	6.83	7.09	0.56	4.29
93160 (O7 V)	7.88	7.95	0.39	4.87
101190 (O7 V)	7.27	7.32	0.37	2.48
168075 (O7 V)	8.77	9.21	0.75	3.53
37041 (O9.5 V)	5.08	4.98	0.20	5.67
149757 (O9.5 V)	2.56	2.58	0.32	2.55
167402 (O9.5 V)	9.03	9.01	0.21	3.38
37021 (B0 V)	7.96	8.20	0.48	5.84
120678 (B0 V)	7.87	8.01	0.44	4.44
199021 (B0 V)	8.43	8.98	0.80	2.98
204827 (B0 V)	7.95	8.75	1.10	2.58
52721 (B2 V)	6.58	6.60	0.30	4.35
93028 (O9.5 V)	8.36	8.30	0.25	2.97
163181 (B1 V)	6.61	6.99	0.70	3.24
46106 (B1 V)	7.93	8.07	0.40	2.79
175876 (O7 V)	6.94	6.84	0.21	3.18
72648 (B1 V)	7.62	7.75	0.38	3.44
96042 (B1 V)	8.23	8.41	0.43	2.01
197512 (B1 V)	8.56	8.62	0.33	2.84
144470 (B1 V)	3.95	3.91	0.22	3.37
209145 (B1 V)	7.62	7.95	0.50	3.37
217979 (B1 V)	8.59	8.94	0.60	2.79
228365 (B1 V)	10.02	10.25	0.46	3.10
14092 (B1 V)	9.23	9.46	0.49	3.15
14422 (B1 V)	9.03	9.53	0.78	2.32
33357 (B1 V)	8.40	8.40	0.26	2.97
41690 (B1 V)	7.71	7.93	0.47	2.91
14357 (B2 II)	8.52	8.84	0.53	2.90

Each dipole responds to the external electric field as well as to the electric field of the other N-1 dipoles that comprise the grain. The polarization at each dipole site is therefore coupled to all other dipoles in the grain. The interaction of all dipoles with the incoming field and with the field of all other dipoles is then obtained by solving $3N \times 3N$ matrix equation, where N is the number of dipoles used to represent the particle volume.

We have used DDA in the first phase to study the light scattering properties of silicates and graphites as individual components. Extinction efficiencies for four silicate grain sizes are shown in Figure 5. The plots also show three spheroids with three different axial ratios (N=9640 with axial ratio AR=1.33; N=25896 with AR=1.50 and N=14440 with AR=2.00). More details on these spheroid generations are given in Vaidya et al. (2007). It is seen that for sizes a=0.1 and 0.2 μ, there seems to be a broad feature seen for all axial ratios.

Figure 6 is for only graphites and here one clearly notices the peak at 2175Å for smaller sizes.

In the second phase of the present study, we have used the DDSCAT6.1 code (Draine & Flatau 2003) which has been modified and developed by Dobbie (1999) to generate the composite grain models. The code, first carves out an outer sphere (or spheroid) from a lattice of dipole sites. Sites outside the sphere are vacuum and sites inside are assigned

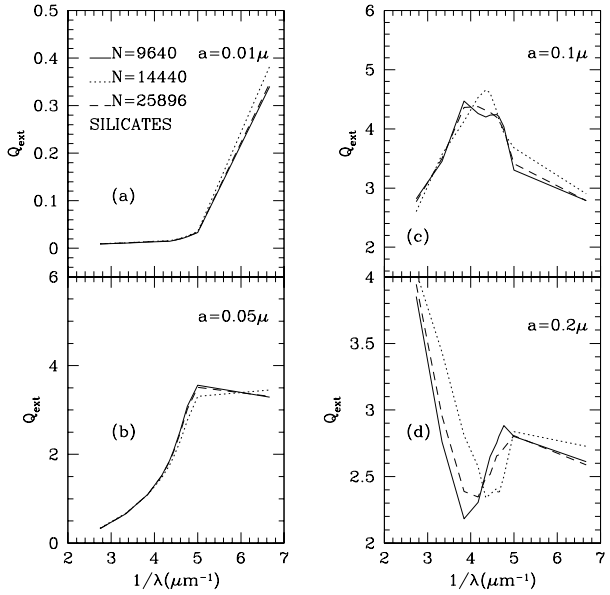

Figure 5. Extinction efficiencies for three spheroidal silicate grains viz. N=9640, 14440 and 25896 dipoles and for four grain sizes; a=0.01, 0.05, 0.1 and 0.5 μ.

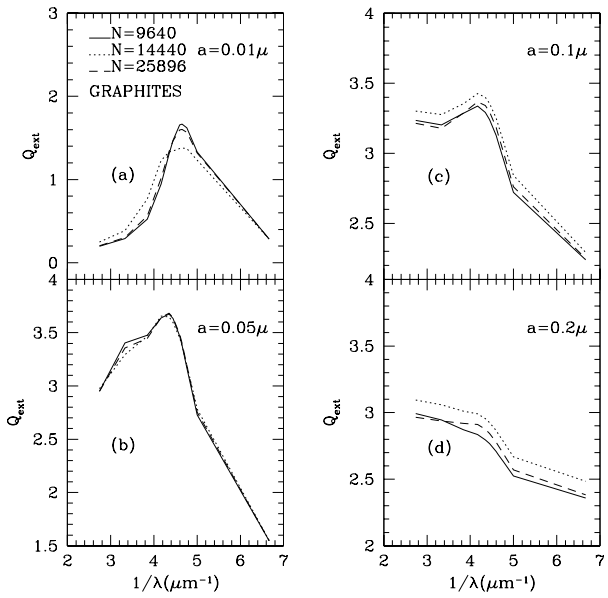

Figure 6. Same as Figure 5 but with spheroidal graphites grains as the component.

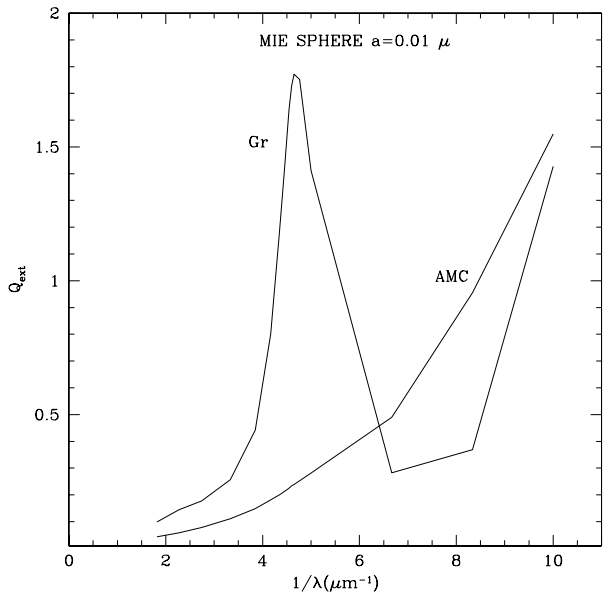

Figure 7. Extinction efficiencies for grains with AMC (Amorphous Carbon) and graphite as the constituent for very small grain size of 0.01μ. The peak in graphite curve at 2175 Å explains why it is being used as inclusion in our composite grain model whereas no such peak is seen in AMC curveat 2175 Å .

to the host material. Once the host grain is formed, the code locates centers for internal spheres to form inclusions. The inclusions are of a single radius and their centers are chosen randomly. The code then outputs a three dimensional matrix specifying the material type at each dipole site which is then received by the DDSCAT program. In the present case, the sites are either silicate, graphite or vacuum.

Many studies of the size distribution have been done over the past few decades, both theoretically and observationally oriented (Oort & van de Hulst 1946; Greenberg 1968; Hong & Greenberg 1978; Mathis et al. 1977; Biermann & Harwit 1980; Mathis 1979; Mathis & Wallenhorst 1981; Mathis & Whiffen 1989). A widely applied size distribution is the one which is proposed by MRN, a power law n(a) $\sim a^{-3.5}$ where a lies between $a_{min} = 0.005\mu$ and $a_{max} = 0.250\mu$ based on the observed diffuse interstellar curve. Zubko et al. (1996, 1998) suggest regularization in which once a grain model is assumed, then a unique size distribution is derived. It is not restricted by any a priori relation such as a power law. However, like most of the other studies above, Zubko et al. use bare spherical grains (astronomical silicate, graphite, AC, SiC, and water ice) and Mie theory to calculate the extinction efficiencies. Graphites and Silicates are most often used in cosmic dust models (see Mathis et al 1977; Draine & Lee 1984, and so on). We have studied the inclusions of graphite and amorphous carbon (AMC) with varied fraction of volume fraction of these inclusions (in a corresponding host spheroid of silicates) as possible candidates for explaining the UV bump feature at 2175Å . Graphite has been a popular candidate as grain constituent for being associated with 2175Å bump feature (Stecher & Donn 1965). These calculations assumed that the graphite or AMC are Mie spheres of size 0.01μ. Figure 7 shows that AMC does not show any peak in extinction efficiency at this wavelength, whereas graphite prominently shows this bump feature. Thus graphite was chosen as the inclusion candidate for this analysis.

In addition to the three axial ratios used for single silicate and graphite individual components, we have used an additional ratio of 4.0 with N=3624 ($48 \times 12 \times 12$) for the composite grain models. The volume fractions of the graphite inclusions used are 10%, 20% and 30% and 40% (denoted as f=0.1, 0.2, 0.3, 0.4) and we have used four different size distributions (i) 0.001-0.100μ (ii) 0.005-0.100μ (iii) 0.005-0.125μ and (iv) 0.005-0.250μ. Details on the computer code and the corresponding modification to the DDSCAT code Draine & Flatau (2003) are given in Dobbie (1999).

Figure 8 and 9 illustrate the composite grain model with number of dipoles N=9640 for the host spheroid and eleven inclusions (152 dipoles per inclusions). Figures 10, 11 and 12 show the basic curves for the three models viz. N=9640, 14440 and 25896 for four different composite grain sizes i.e. 0.01, 0.05, 0.1, 0.2 μ. The variation of fraction f in Graphite concentration causes variation in width of the extinction bump (Vaidya et al. 2001; Gupta et al. 2006). We have varied the fraction from 0.1 to 0.4 for N=9640 and N=14440 and f=0.1 to 0.3 for N=25896. It is clearly seen that extinction curves vary considerably with size and infact "2175Å " feature is clearly seen for small grains ; viz. a=0.01 and 0.05 μ. This feature was also observed by Vaidya et al. (2007) and was extended to f=0.4 in the present work. Moreover, Vaidya & Gupta (1997) and Vaidya & Gupta (1999) have found the variation in '2175Å ' bump feature (shape and peak wavelength shift) with the variation in the porosity of the grains. Table 4 shows the number of dipoles for each grain model and number of dipoles per inclusion with the number of inclusions for each fraction.

Table 4. Number of dipoles for each inclusion (number of inclusions is shown in brackets) for the four models

No. of Dipoles (Axial ratio)	f=0.1	f=0.2	f=0.3	f=0.4
N=9640(1.33)	152(6)	152(11)	152(16)	152(21)
N=25896(1.50)	432(7)	432(13)	432(19)	-
N=14440(2.00)	224(6)	224(11)	224(16)	221(21)
N=3624(4.00)	136(3)	136(6)	69(9)	-

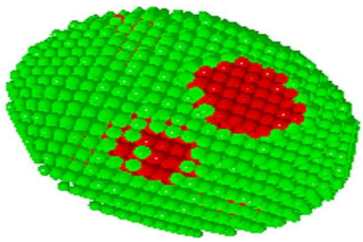

Figure 8. A non-spherical composite dust grain with a total of N=9640 dipoles where the inclusions embedded in the host spheroid are shown such that only the ones placed at the outer periphery are seen.

4 RESULTS AND DISCUSSIONS

Figures 10, 11 and 12 show the basic Q_{ext} curves for three axial ratios and four volume fractions of graphite inclusions. For all the three models a shift in peak wavelength is seen as the volume fraction of inclusion increases. Further, the extinction efficiency also varies with the change in volume fraction.

Each individual IUE observed extinction curve is compared with with the model curve formed from a χ^2 minimized and best fit linear combination of the composite

Figure 9. Same as Figure 8 but showing the inclusions.The fraction of Graphite inclusions is 20%. The no. of inclusions are 11 with 152 dipoles per inclusions.

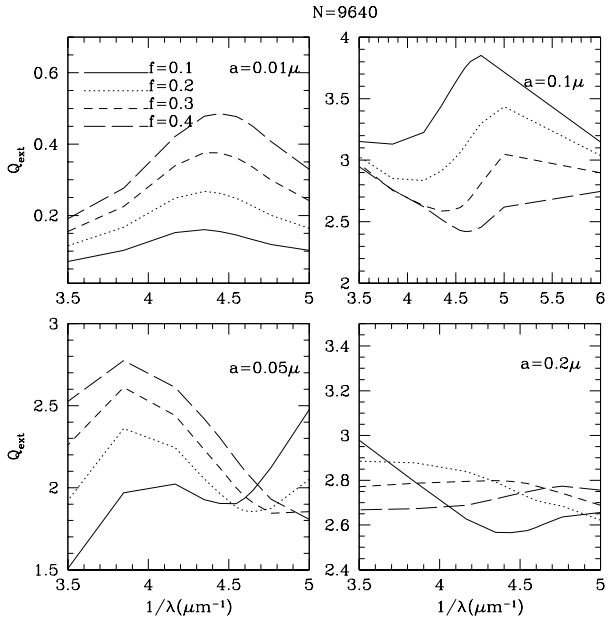

Figure 10. Extinction efficiency for the composite grains, with N=9640 for four volume fraction of inclusions, f=10%, 20%, 30% & 40%.

grains (contributory fraction p) and solid graphite grains (contributory fraction q); i.e the model interstellar extinction curves for the composite grains and the graphite grains are linearly combined to render a net curve for comparison with the observed extinction curve for the various stars.The formula to obtain the minimized χ^2 values is given by Bevington (1969).

$$\chi_j^2 = \frac{1}{pp} \frac{\sum_{i=1}^{n} (S_i^j - T_i^k)^2}{\sum_{i=1}^{n} \sigma_i^2}$$

where pp is the degrees of freedom, $S_i^j(\lambda_i)$ is the jth model curve for the corresponding x and y linear combination of composite and graphite grains and $T_i^k(\lambda_i)$ is for the observed curve, λ_i are the wavelength points with i=1,n where n are the number of wavelength points of the extinction curves and σ_i is the standard deviation which is depicted as error bars in Figure 13, 14, 15, 16 & 17.

Table 5 shows (i) HD number of the program star (ii) the best fit χ^2 values (iii) fractional contribution 'p' of Si+f*Gr and (iv) 'q' of the solid Graphite, (v) no. of dipoles N (vi) graphite fraction 'f' of composite grain (vii) corresponding grain size distribution of the best fit model (viii) and observed R_v for the star sorted in ascending order of its values.

Fig 13, 14, 15 & 16 show the comparison of the observed interstellar extinction curve with the best fit model combination curve of composite grains and graphite grains in the wavelength range of 0.3650-0.1500μm.

Figure 17 shows the fitting for four selected sight lines with R_v values ranging from 2.14 to 5.67. It is easy to see that the height of the UV bump decreases significantly with an increase of R_v.

Table 5. Best fit table for stars whose extinction curves were generated using Pair Method and FM method.

HD STAR #	χ^2	p	q	N	f_{Gr}	a(μ)	Obs. R_v
96042	0.49040	0.5	0.3	14440	0.1	0.005-0.100	2.01
198781	0.45582	0.5	0.4	14440	0.1	0.005-0.100	2.14
14422	2.72753	0.3	0.4	14440	0.1	0.001-0.100	2.32
101190	0.46696	0.3	0.3	14440	0.1	0.001-0.100	2.48
185418	10.5079	0.2	0.5	14440	0.1	0.001-0.100	2.54
149757	0.17317	0.3	0.4	14440	0.1	0.001-0.100	2.55
204827	6.64334	0.6	0.3	14440	0.1	0.005-0.100	2.58
18352	4.9040	0.2	0.5	14440	0.1	0.005-0.100	2.66
13338	1.06889	0.3	0.5	14440	0.1	0.001-0.100	2.75
1383	2.4113	0.4	0.4	14440	0.1	0.005-0.250	2.77
24432	17.7614	0.3	0.5	14440	0.1	0.001-0.100	2.77
217979	0.81775	0.3	0.4	14440	0.1	0.001-0.100	2.79
46106	0.64620	0.4	0.4	14440	0.1	0.005-0.250	2.79
217086	8.9350	0.2	0.4	14440	0.1	0.001-0.100	2.80
46660	8.9930	0.2	0.5	14440	0.1	0.005-0.100	2.82
197512	0.30716	0.3	0.5	14440	0.1	0.001-0.100	2.84
14357	0.72808	0.5	0.4	14440	0.1	0.005-0.100	2.90
41690	0.98679	0.5	0.4	14440	0.1	0.005-0.100	2.91
198478	3.9900	0.2	0.4	14440	0.1	0.001-0.100	2.93
33357	0.30627	0.4	0.5	14440	0.1	0.005-0.100	2.97
93028	0.11806	0.4	0.3	14440	0.1	0.005-0.125	2.97
199021	0.64667	0.6	0.3	25896	0.1	0.005-0.125	2.98
38131	5.2845	0.3	0.3	14440	0.1	0.001-0.100	3.01
217061	8.7446	0.3	0.4	14440	0.1	0.005-0.100	3.03
228365	0.74083	0.3	0.4	14440	0.1	0.001-0.100	3.10
46202	5.2634	0.3	0.3	14440	0.1	0.001-0.100	3.12
216658	18.7932	0.4	0.4	14440	0.1	0.005-0.250	3.14
14092	1.62061	0.5	0.4	14440	0.1	0.005-0.100	3.15
175876	0.11746	0.6	0.3	14440	0.1	0.005-0.250	3.18
326330	0.71815	0.4	0.4	14440	0.1	0.005-0.100	3.18
47240	7.1508	0.2	0.3	14440	0.1	0.001-0.100	3.22
163181	1.37851	0.6	0.4	14440	0.1	0.005-0.250	3.24
13854	3.2980	0.4	0.4	14440	0.1	0.005-0.250	3.29
225094	12.1601	0.2	0.4	14440	0.1	0.001-0.100	3.29
123008	4.2513	0.3	0.4	14440	0.1	0.001-0.100	3.32
152667	1.3020	0.4	0.3	14440	0.1	0.005-0.100	3.33
152723	2.7402	0.2	0.3	14440	0.1	0.001-0.100	3.36
144470	0.18836	0.3	0.5	14440	0.1	0.005-0.250	3.37
209145	1.05961	0.6	0.4	14440	0.1	0.005-0.250	3.37
167402	0.19020	0.6	0.3	14440	0.1	0.005-0.100	3.38
167838	2.6239	0.3	0.4	14440	0.1	0.005-0.100	3.39
34078	1.0951	0.2	0.4	14440	0.1	0.001-0.100	3.42
72648	0.49959	0.5	0.4	14440	0.1	0.005-0.250	3.44
43818	5.1926	0.2	0.4	14440	0.1	0.001-0.100	3.46
164816	1.0931	0.3	0.3	14440	0.1	0.005-0.100	3.52
168075	2.11725	0.4	0.4	14440	0.1	0.005-0.250	3.53
252325	44.2798	0.2	0.4	14440	0.1	0.005-0.125	3.55
37367	0.9525	0.2	0.5	14440	0.1	0.001-0.100	3.55
122669	22.9634	0.4	0.4	14440	0.1	0.005-0.250	4.09
37903	0.6400	0.3	0.3	14440	0.1	0.005-0.100	4.11
93632	1.4302	0.4	0.3	14440	0.1	0.005-0.250	4.17
37061	1.01083	0.3	0.2	14440	0.3	0.005-0.100	4.29
52721	0.29883	0.4	0.4	14440	0.1	0.005-0.100	4.35
120678	0.33590	0.3	0.3	14440	0.1	0.005-0.250	4.44
93222	2.6560	0.3	0.2	9640	0.2	0.001-0.100	4.76
37023	0.61695	0.2	0.2	14440	0.3	0.005-0.100	4.82
93160	0.47897	0.6	0.4	14440	0.1	0.005-0.250	4.87
37041	0.22975	0.4	0.2	14440	0.3	0.005-0.100	5.67
37021	0.23386	0.1	0.1	14440	0.1	0.001-0.100	5.84

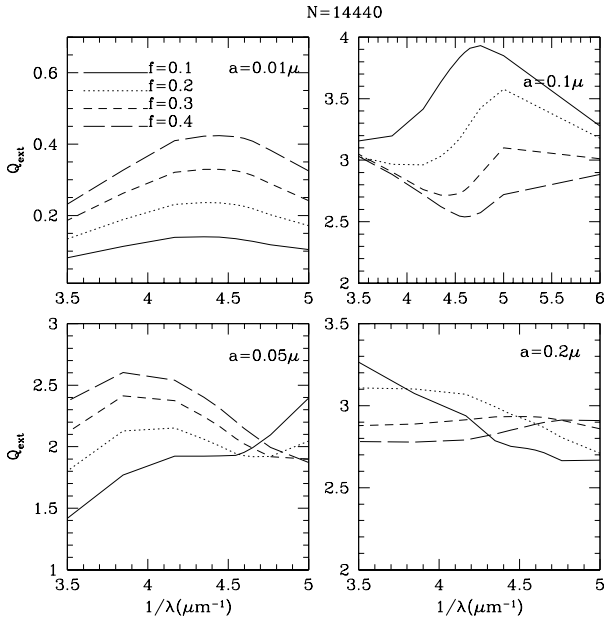

Figure 11. Same as Fig 11 but for N=14440.

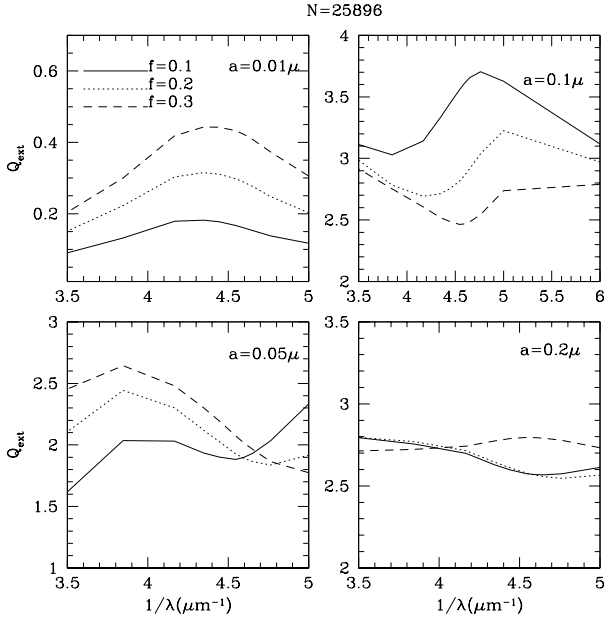

Figure 12. Same as Fig 11 but for N=25896 and three volume fraction of inclusions viz. f=10%, 20%, 30% & 40%.

4.1 Error Analysis

Set I:

We use notation $k(\lambda-V)$ for the normalised extinction $E(\lambda-V)/E(B-V)$. Let $K(\lambda-V)$=$\Delta m(\lambda-V)/\delta(B-V)$ and considering only random error measurements in these variables, propagation of error analysis gives (Massa et al. 1983):

$$\sigma[k(\lambda-V)] = \sqrt{2}\frac{(\sigma[m(\lambda-V)]^2 + k(\lambda-V)^2\sigma(B-V)^2)^{1/2}}{\Delta(B-V)} \quad (4)$$

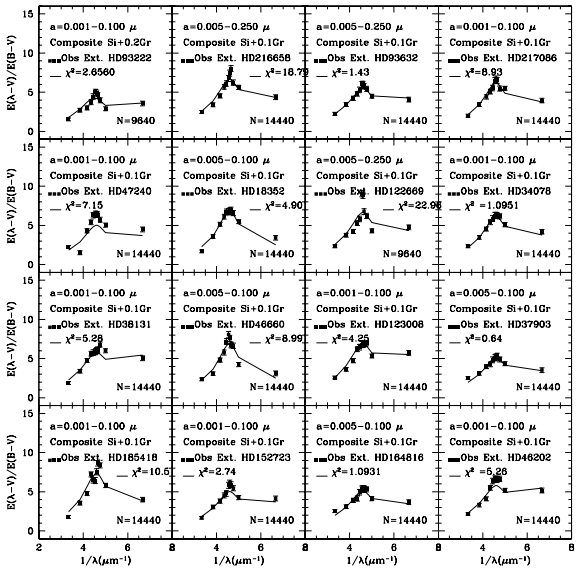

Figure 13. Comparison of the observed interstellar extinction with the best fit model in the wavelength range 0.3650-0.15004μm. The dots are the observed data for the extinction curve generated using "Pair method" (Set I).

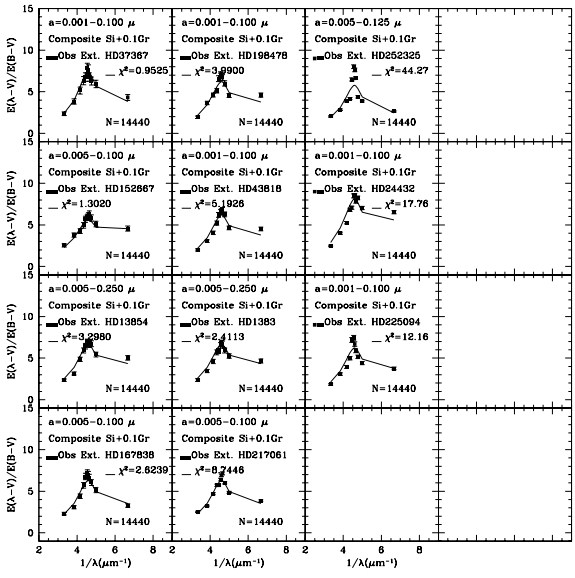

Figure 14. same as Fig 13.

where $\sigma[m(\lambda-V)]$ is a systematic shift in the zero point of an IUE camera image described by Bohlin et al. (1980) which is about 0.03mag. $\sigma(B-V)$ is taken to be 0.015mag and $\Delta(B-V)$ is the difference in the intrinsic (B-V) colors of the reddened and the unreddened stars.

Set II:

Here again, the notation $k(\lambda-V)$ is used for the nor-

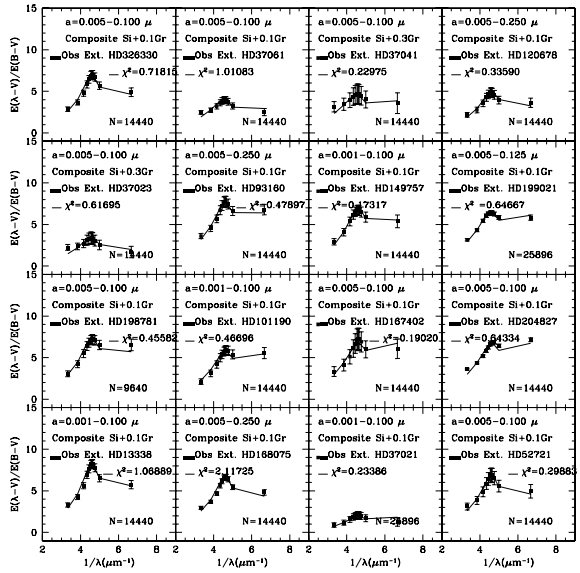

Figure 15. Comparison of the observed interstellar extinction with the best fit model in the wavelength range 0.3650-0.1500μm. The dots are the observed data for the extinction curve generated using FM Method (Set II).

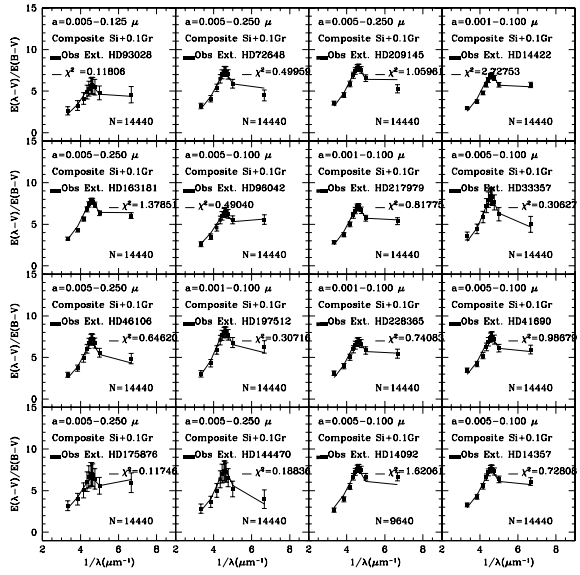

Figure 16. same as Fig 15.

malised extinction $E(\lambda - V)/E(B - V)$. As, the normalised extinction is given by equation (3), the error in $k(\lambda - V)$ is given by:

$$\sigma[k(\lambda-V)] = [\sigma_{c_1}^2 + x^2\sigma_{c_2}^2 + D^2\sigma_{c_3}^2 + c_3^2[(\frac{\partial D}{\partial x_o})^2\sigma_{x_o}^2 + (\frac{\partial D}{\partial \gamma})^2\sigma_\gamma^2] + \sigma_F^2 F_{is}]^{1/2} \quad (5)$$

The empirical uncertainties in extinction curve coefficients (σ's) are derived from Table 7 of Fitzpatrick & Massa (1990).

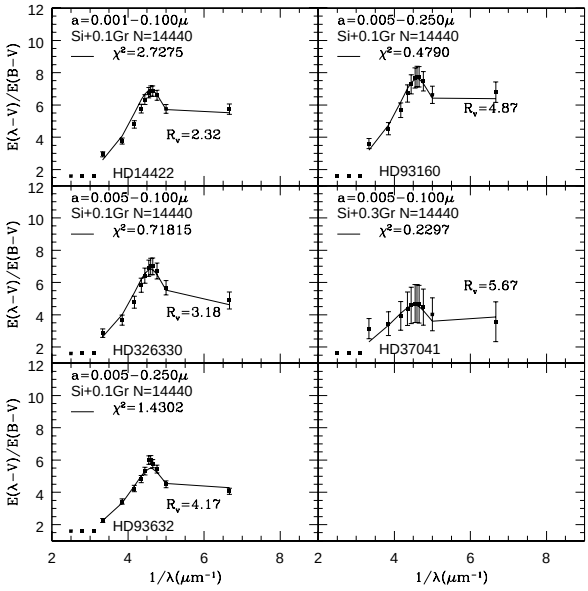

Figure 17. Best fit curves for different stars having R_v values viz. 2.14, 3.18, 4.35 ,4.87 & 5.67.

However, we ignore the first term on the right hand side of above equation as χ^2 minimization at each data point should be independent of each other and this term adds an normalization constant to the whole equation.

We see that the normalization during error analysis is done with $\Delta(B - V)$ (Set I) and E(B-V) (Set II). We have E(B-V) for the 59 sample stars ranging from as low as 0.20 to very high value 1.10. This normalization is the main cause for variation in the errors in both the cases. Thus we see that the stars having low E(B-V) have larger errors and hence very low χ^2 values and vice-versa for the stars having high E(B-V) values.

The following results are obtained:

(1) The extinction efficiencies of individual silicate and graphite grains show changes in the efficiency curves with change in axial ratios as well as sizes. A prominent 2175Å feature is seen for smaller graphite grains.

(2) It has been found that solid graphite grains are responsible for the bump feature at 2175Å and we have shown that other forms of carbon for eg. AMC (Amorphous Carbon) does not show this particular feature. However, AMC shows a absorption peak around 2500-3000Å but not at 2175Å .

(3) Having obtained the basic curves for different models for different sizes viz. a=0.01, 0.05, 0.1, 0.2 μ we conclude that a variation is seen in the extinction values as the fraction of the graphite varies. It is seen that for small grains, (viz. 0.01 and 0.05) extinction efficiency increases with increase in volume fraction. A peak is seen at '2175Å ', which is more prominent for sizes 0.05 and 0.1 μ viz. Figures 10, 11 and 12. There is a shift in peak wavelength seen in these curves. The extinction feature at '2175Å ' seems to shift

towards longer wavelengths with the volume fraction of inclusions.

(4) The model extinction curves with composite spheroidal grains having axial ratio of AR=2.00 (N=144440) and graphite inclusion fraction of 10% seems to fit reasonably well with most of the directions in the galaxy for the stars whose extinction curves were derived using "Pair Method" and "FM Method". The results are shown in Table 5.

(5) R_v which is defined by $R_v = A(V)/E(B-V)$ is one parameter which can describe the interstellar conditions towards a particular star's line of sight. R_v tends to be higher in dense clouds where grains grow by coagulation because of higher extinction due to more number of dust grains whereas R_v tends to be lower in diffuse environment. Results for the composite grain models show that small size distribution of grains i.e 0.001-0.100μm and 0.005-0.100μm provide a better fit for low R_v directions ($\sim$ 2 to 3) and for large size distribution 0.005-0.250μm, better fits are found for R_v directions in the range $\sim$4-6 in most of the cases. Deviation from the average extinction curves for a given R_v must provide additional important empirical clues to the evolutionary processes (Clayton & Mathis 1988; Cardelli & Clayton 1991; Mathis & Cardelli 1992; Jenniskens 1993).

5 CONCLUSIONS

The major conclusion from this study can be summarized as follows:

(i) Small sized graphite grains are an important component for the composite dust grains to reproduce the UV bump at '2175Å ' of interstellar extinction curves whereas amorphous carbon does not seem to reproduce this feature.

(ii) There is a good correlation of the strength of the bump feature with the varying R_v values i.e. the strength decreases with an increase in the R_v. The main reason for this is due to variation in grain size distribution with environment which varies the R_v and hence the strength of the observed bump feature. Variation in size distribution seen by this work indicates that small grains coagulate onto large grains in relatively dense environments, as expected (Draine & Anderson 1985; Draine 1990).

(iii) The spheroidal composite grain with the axial ratios not very large (1.33-2.0) reasonably fit most of the observed IUE data analysed in the present study.

(iv) Our study indicates that small grains might be responsible for the sight lines with low R_v values i.e. in diffuse dust regions; whereas larger grains could be responsible in the regions of dense clouds where R_v is higher which is in consistency with Kim et.al (1994).

Further work is in progress to estimate the abundances of interstellar carbon in various sight lines which may provide more insight into the dust grain evolution etc.

6 ACKNOWLEDGMENTS

We acknowledge ISRO-RESPOND project for funding this research. R. Misra of IUCAA helped in formulating the error analysis and we owe thanks to him.

REFERENCES

Aiello S., Barsella B., Chlewicki G., Greenberg J. M., Patriarchi P., Perinotto M., 1988, in ESA Special Publication, Vol. 281, ESA Special Publication, pp. 223–226
Biermann P., Harwit M., 1980, ApJ, 241, L105
Bohlin R. C., Sparks W. M., Holm A. V., Savage B. D., Snijders M. A. J., 1980, A&A, 85, 1
Cardelli J. A., Clayton G. C., 1991, AJ, 101, 1021
Cardelli J. A., Clayton G. C., Mathis J. S., 1988, ApJ, 329, L33
Clayton G. C., Mathis J. S., 1988, ApJ, 327, 911
Clayton G. C., Wolff M. J., Sofia U. J., Gordon K. D., Misselt K. A., 2003, ApJ, 588, 871
Draine B. T., 1988, ApJ, 333, 848
—, 1990, in Astronomical Society of the Pacific Conference Series, Vol. 12, The Evolution of the Interstellar Medium, L. Blitz, ed., pp. 193–205
Draine B. T., Anderson N., 1985, ApJ, 292, 494
Draine B. T., Flatau P. J., 2003, ArXiv Astrophysics e-prints
Draine B. T., Goodman J., 1993, ApJ, 405, 685
Fitzpatrick E. L., Massa D., 1986, ApJ, 307, 286
—, 1988, ApJ, 328, 734
—, 1990, ApJS, 72, 163
—, 2005, AJ, 130, 1127
—, 2007, ApJ, 663, 320
—, 2009, ApJ, 699, 1209
Greenberg J. M., 1968, Interstellar Grains, Middlehurst, B. M. & Aller, L. H., ed., the University of Chicago Press, pp. 221–+
Greenberg J. M., Chlewicki G., 1983, ApJ, 272, 563
Gupta R., Vaidya D. B., Bobbie J. S., Chylek P., 2006, Ap&SS, 301, 21
Hong S. S., Greenberg J. M., 1978, A&A, 70, 695
Jenniskens P., 1993, A&A, 274, 653
Kim S., Martin P. G., Hendry P. D., 1994, ApJ, 422, 164
Massa D., Savage B. D., Cassinelli J. P., 1984, ApJ, 287, 814
Massa D., Savage B. D., Fitzpatrick E. L., 1983, ApJ, 266, 662
Mathis J. S., 1979, ApJ, 232, 747
Mathis J. S., Cardelli J. A., 1992, ApJ, 398, 610
Mathis J. S., Rumpl W., Nordsieck K. H., 1977, ApJ, 217, 425
Mathis J. S., Wallenhorst S. G., 1981, ApJ, 244, 483
Mathis J. S., Whiffen G., 1989, ApJ, 341, 808
Meyer D. M., Savage B. D., 1981, ApJ, 248, 545
Oort J. H., van de Hulst H. C., 1946, Bull. Astron. Inst. Netherlands, 10, 187
Stecher T. P., Donn B., 1965, ApJ, 142, 1681
Vaidya D. B., Gupta R., 1997, A&A, 328, 634
—, 1999, A&A, 348, 594
Vaidya D. B., Gupta R., Dobbie J. S., Chylek P., 2001, A&A, 375, 584
Vaidya D. B., Gupta R., Snow T. P., 2007, MNRAS, 379, 791
Valencic L. A., Clayton G. C., Gordon K. D., 2004, ApJ, 616, 912

Voshchinnikov N. V., Il'in V. B., Henning T., 2005, A&A, 429, 371
Voshchinnikov N. V., Il'in V. B., Henning T., Dubkova D. N., 2006, A&A, 445, 167
Weingartner J. C., Draine B. T., 2001, Apj, 548, 296
Wolff M. J., Clayton G. C., Gibson S. J., 1998, ApJ, 503, 815
Wolff M. J., Clayton G. C., Martin P. G., Schulte-Ladbeck R. E., 1994, ApJ, 423, 412
Wu C., Ake T. B., Boggess A., Bohlin R. C., Imhoff C. L., Holm A. V., Levay Z. G., Panek R. J., Schiffer III F. H., Turnrose B. E., 1983, NASA IUE Newsl., No. 22, 2+324 pp., 22
Zubko V. G., Krełowski J., Wegner W., 1996, MNRAS, 283, 577
Zubko V. G., Krelowski J., Wegner W., 1998, MNRAS, 294, 548